

Composite AdS geodesics for CFT correlators and timelike entanglement entropy

Hardik Bohra¹ and Allic Sivaramakrishnan²

¹*Department of Physics and Astronomy, University of Kentucky, Lexington, KY 40506*

²*Walter Burke Institute for Theoretical Physics, California Institute of Technology, Pasadena, CA 91125*

We study how to recover timelike worldlines in AdS from CFT data as a toy model for holographically reconstructing realistic observers. We give a bulk extremization procedure that determines composite timelike-spacelike geodesics that connect timelike-separated boundary points. The total geodesic length matches the length extracted from CFT correlators at the timelike-separated points. We show agreement in Poincaré AdS, for generic boundary points in global AdS, and also for the BTZ solution, in which the timelike segment probes behind the horizon. We refine related methods to compute timelike entanglement entropy in AdS₃/CFT₂ and recover known results.

I. INTRODUCTION

Holography offers a well-controlled way to study observers and observables in quantum gravity. Approaches to bulk reconstruction focus on recovering field operators in anti-de Sitter space (AdS) from the dual conformal field theory (CFT). Methods include HKLL reconstruction [1, 2], ideas arising from the Ryu-Takayanagi formula [3, 4], and work on recovering operators within the black hole interior [5–7]. Graviton contributions are challenging to include in these approaches, but are more easily incorporated if we model a realistic observer by its worldline, and measurements by operator insertions along the worldline (see [8] for a review).

CFT correlation functions capture bulk effective field theory [9–19] and can probe the black hole interior [5, 20–28] via, in the simplest settings, the geodesic or WKB approximation: the Euclidean vacuum two-point function of a scalar ϕ with mass m behaves as $\langle \phi(x_1)\phi(x_2) \rangle \sim e^{-m\ell(x_1, x_2)}$ for $m\ell(x_1, x_2) \gg 1$, with geodesic distance $\ell(x_1, x_2)$. In this regime, CFT correlators at spacelike separations are computed by boundary-anchored spacelike geodesics. Whether something similar happens for timelike separations is less clear, as AdS does not have boundary-anchored timelike geodesics (but see [29–35]).

However, timelike entanglement entropy [36–38] in the CFT is computed in AdS by composite codimension-two extremal surfaces, and in AdS₃/CFT₂ these are chains of timelike and spacelike geodesics that connect two timelike-separated boundary points. The geometry and surfaces are sometimes complexified [36, 37, 39, 40], raising questions about extensions to non-analytic setups.

Here, we give a prescription for determining composite, real geodesics that connect timelike-separated boundary points x_1, x_2 in AdS _{$d+1$} /CFT _{d} in the original geometry:

1. Compute the total proper length ℓ_s of geodesics that connect boundary points x_1, x_2 to bulk points y_1, y_2 respectively, and the proper time ℓ_t of a geodesic between y_1, y_2 .

2. Extremize ℓ_s, ℓ_t over y_1, y_2 .

3. To fix any remaining degeneracy, compare $\ell_s + i\ell_t$ to $\ell(x_1, x_2)$ obtained by analytically continuing x_1, x_2 to timelike separations with a specific $i\epsilon$ prescription that we give.

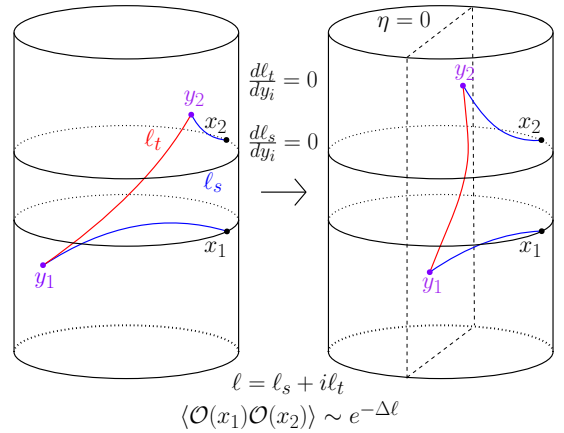


FIG. 1. For timelike-separated boundary points x_1, x_2 , we extremize the lengths ℓ_s, ℓ_t over bulk points y_1, y_2 . We show this uniquely specifies a composite geodesic whose complex length ℓ is equal to the length extracted from $\langle \mathcal{O}(x_1)\mathcal{O}(x_2) \rangle$.

We find that this prescription, depicted in Figure (1), determines composite geodesics with a unique complex length $\ell(x_1, x_2)$. We further show that $\ell(x_1, x_2)$ matches the length extracted from time-ordered boundary two-point functions $\langle \mathcal{O}(x_1)\mathcal{O}(x_2) \rangle$.

Our results reproduce timelike entanglement entropy in AdS₃/CFT₂. Our prescription refines the approaches in [36, 37, 39, 40] by using only the original, uncomplexified geometry and its geodesics, and by making no assumptions about the points that join the segments.

We compute $\ell(x_1, x_2)$ in Poincaré AdS in Section II, in global AdS for generic x_1, x_2 in Section III, and in the BTZ solution in Section IV. We confirm our results by studying the geodesics themselves in Appendices A and B. In Appendix C, we review how proper time differs from modular time.

bohra.hardik@uky.edu, allic@caltech.edu

II. POINCARÉ ADS

AdS admits geodesics that connect boundary points x_1, x_2 when they are spacelike separated, but not when timelike separated. However, working in Poincaré AdS, we will analyze solutions to the geodesic equation and find that timelike-separated boundary points x_1, x_2 can indeed be connected by a composite geodesic—a curve composed of concatenated timelike and spacelike geodesic segments. For definiteness, we consider AdS₃/CFT₂, although our results apply trivially to AdS_{d+1}/CFT_d. The metric is

$$ds^2 = \frac{1}{z^2}(-dt^2 + dw^2 + dz^2), \quad (1)$$

where $z = 0$ is the AdS boundary, and we set $R_{AdS} = 1$. The boundary points are $x_i = (t_i, w_i)$ and the bulk points $y_i = (t_i, w_i, z_i)$.

We first consider the spacelike configuration $(x_1 - x_2)^2 > 0$. We parameterize bulk curves between x_1 and x_2 by an affine parameter λ normalized such that the velocity $\dot{y}^\mu \equiv (\dot{t}, \dot{w}, \dot{z})$ obeys $\dot{y}^\mu \dot{y}_\mu = 1$. The geodesic equations are

$$\dot{t} = Ez^2, \quad \dot{w} = Pz^2, \quad \dot{z}^2 = z^2(1 - Q^2z^2), \quad (2)$$

where E, P and $Q^2 = -E^2 + P^2$ are constants of motion determined by boundary data, $Q^{-2} = \frac{1}{4}(x_1 - x_2)^2$. Equation (2) shows that the geodesic, which is a semicircle, has a turning point in z . We can solve (2) with the AdS boundary located at $\lambda = \pm\infty$.

To compute the geodesic length $\ell(x_1, x_2)$, we introduce a cutoff surface at $z = \delta \ll 1$. The boundary is then located at $\pm\lambda_{\max}$ and we recover the familiar length formula, $\ell = 2\lambda_{\max} = \log((x_1 - x_2)^2/\delta^2)$.

Now, we analytically continue ℓ in x_1, x_2 to reach the timelike configuration $(x_1 - x_2)^2 < 0$. For reasons that will become clear, of the two possible continuations, we choose the one in which ℓ acquires a positive imaginary contribution,

$$\ell = i\pi + 2 \log\left(\sqrt{(t_1 - t_2)^2 - (w_1 - w_2)^2/\delta^2}\right). \quad (3)$$

Whether this ℓ is the length of some curve is now unclear.

We can in fact show that $\ell = i\ell_t + \ell_s$ is the length of a bulk curve connecting x_1 and x_2 that is a union of a timelike geodesic with length ℓ_t and two spacelike geodesics with total length ℓ_s . For timelike-separated boundary points, the boundary-anchored spacelike segments described by equation (2) have $Q^2 < 0$, which implies that $z(\lambda)$ has no turning point. The spacelike geodesics anchored at x_1 and x_2 therefore originate at $z = \delta$ and reach the Poincaré horizons, $z = \infty$ with $t = \pm\infty$. This was found in [36, 37].

We can further identify a timelike geodesic between the horizons. Setting $w_1 = w_2$ for simplicity, a timelike geodesic in the Poincaré patch parameterized by $\tau \in [-\pi/2, \pi/2]$ with $\dot{y}^\mu \dot{y}_\mu = -1$ satisfies $-\dot{t}^2 + \dot{z}^2 =$

$-z^2$ and $\dot{t} = p_t z^2$. Its solution $(t(\tau), w_1, z(\tau))$ satisfies $z^2 - (t - t_0)^2 = p_t^{-2}$ for constants t_0 and p_t . From this, we can see that timelike geodesics cannot reach the boundary for finite p_t : as $\dot{z}^2 = z^2(p_t^2 z^2 - 1)$, the region $z < 1/p_t$ is forbidden.

The length ℓ_t of this geodesic is

$$\ell_t = 2 \int_{1/p_t}^{\infty} \frac{dz}{z\sqrt{p_t^2 z^2 - 1}} = \pi. \quad (4)$$

The same result holds for $w_2 - w_1 \neq 0$. The length is independent of p_t , and so there is a family of distinct geodesics parameterized by p_t , whose value does not appear to be fixed by boundary conditions.

For comparison, the time-ordered CFT two-point function of two primaries is $\langle 0|\mathcal{O}(x_1)\mathcal{O}(x_2)|0\rangle = 1/((x_1 - x_2)^2 + i\epsilon)^\Delta$, and in the spacelike configuration,

$$\ell = -\frac{1}{\Delta} \log \langle 0|\mathcal{O}(x_1)\mathcal{O}(x_2)|0\rangle = \log((x_1 - x_2)^2 + i\epsilon). \quad (5)$$

Analytically continuing to timelike separations gives

$$\ell = \log(|x_1 - x_2|^2) + i\pi = \ell_s + i\ell_t, \quad (6)$$

in agreement with the geodesic calculation we provided. Note that the time-ordered two-point function corresponds to a specific $i\epsilon$ prescription that gives $i\pi$ regardless of the sign of $t_1 - t_2$. This choice of $i\epsilon$ specifies the analytic continuation of the length, which we will take as the definition of this continuation from now on.

III. GLOBAL ADS

In global AdS coordinates, the extremization prescription summarized in the introduction produces a unique piecewise-geodesic curve between x_1, x_2 . We work in global AdS₃, but our results apply without loss of generality to AdS_{d+1}. The metric is

$$ds^2 = -\cosh^2\rho dt^2 + d\rho^2 + \sinh^2\rho d\phi^2, \quad (7)$$

where $\rho \geq 0$ and the AdS boundary is located at $\rho = \infty$. The geodesic distance between bulk points in AdS can be expressed in embedding-space coordinates. For the embedding space $\mathbb{R}^{2,2}$, with metric $\text{diag}(-1, -1, 1, 1)$, the AdS geodesic distance between points X_I and X_J is

$$\cosh L = X_I^0 X_J^0 + X_I^1 X_J^1 - X_I^2 X_J^2 - X_I^3 X_J^3. \quad (8)$$

To exploit the symmetries of the setup, we change coordinates to an AdS₂ slicing of global AdS₃ (see, for example [37]),

$$ds^2 = d\eta^2 + \cosh^2(\eta)(-\cosh^2(r)dt^2 + dr^2), \quad (9)$$

with $-\infty < \eta, r < \infty$, and where $\eta = \pm\infty$ is the boundary. The relation to embedding space is

$$\begin{aligned} X^0 &= \cosh(\eta) \cosh(r) \sin(t), & X^2 &= \sinh(\eta), \\ X^1 &= \cosh(\eta) \cosh(r) \cos(t), & X^3 &= \cosh(\eta) \sinh(r). \end{aligned} \quad (10)$$

Following (8) and (10), the geodesic distance is

$$\cosh L = \cosh \eta_1 \cosh \eta_2 (\cosh r_1 \cosh r_2 \cos(t_1 - t_2) - \sinh r_1 \sinh r_2) - \sinh \eta_1 \sinh \eta_2. \quad (11)$$

The geodesic distance between boundary points $x_1 = (T_1, R_1)$ and $x_2 = (T_2, R_2)$ is

$$\ell = \log \left[\frac{1}{2\delta^2} \left(-1 + \cosh R_1 \cosh R_2 \cos(T_1 - T_2) - \sinh R_1 \sinh R_2 \right) \right], \quad (12)$$

with radial cutoff $\delta = \exp(-\eta_\infty)$. The boundary is AdS_2 , which implies that the boundary light cone is defined by where the logarithm's argument in (12) vanishes. Analytically continuing $\cosh L$ from the spacelike to timelike configuration therefore gives

$$\ell = i\pi + \log \left[\left(1 - \cosh R_1 \cosh R_2 \cos(T_1 - T_2) + \sinh R_1 \sinh R_2 \right) / (2\delta^2) \right]. \quad (13)$$

This agrees with the length extracted in the usual way from the vacuum two-point function, $\ell = -(1/\Delta) \log \langle \mathcal{O}(R_1, T_1) \mathcal{O}(R_2, T_2) \rangle$ in global coordinates at timelike separations.¹

We now apply our prescription to identify a boundary-anchored bulk curve whose length is (13). We first focus on a bulk-to-bulk timelike geodesic. Denoting the endpoints that solve the extremization conditions as $(\boldsymbol{\eta}_1, \mathbf{t}_1, \mathbf{r}_1)$ and $(\boldsymbol{\eta}_2, \mathbf{t}_2, \mathbf{r}_2)$, we extremize (11),

$$\frac{dL}{d\eta_1} = \frac{dL}{d\eta_2} = \frac{dL}{dt_1} = \frac{dL}{dr_1} = \frac{dL}{dt_2} = \frac{dL}{dr_2} = 0. \quad (14)$$

Solving $\frac{dL}{d\eta_i} = 0$ gives $\boldsymbol{\eta}_1 = \boldsymbol{\eta}_2 = 0$, for which

$$\begin{aligned} \frac{dL}{dr_1} &= \sinh r_1 \cosh r_2 \cos(t_1 - t_2) - \cosh r_1 \sinh r_2, \\ \frac{dL}{dt_1} &= -\cosh r_1 \cosh r_2 \sin(t_1 - t_2), \\ \frac{dL}{dr_2} &= \cosh r_1 \sinh r_2 \cos(t_1 - t_2) - \sinh r_1 \cosh r_2, \\ \frac{dL}{dt_2} &= \cosh r_1 \cosh r_2 \sin(t_1 - t_2). \end{aligned} \quad (15)$$

Solving $dL/dt_i = 0$ gives $t_1 - t_2 = n\pi$. In this case, $dL/dr_i = 0$ yields $\tanh r_1 = (-1)^n \tanh r_2$. Altogether, we have

$$\mathbf{t}_1 - \mathbf{t}_2 = n\pi, \quad \mathbf{r}_1 = (-1)^n \mathbf{r}_2, \quad n \in \mathbb{Z}. \quad (16)$$

¹To see this, note that in embedding space, $\langle \mathcal{O}(P_1) \mathcal{O}(P_2) \rangle = 1/(-P_1 \cdot P_2)^\Delta$ with projective boundary points $P_i = (\cosh R_i \sin T_i, \cosh R_i \cos T_i, 1, \sinh R_i)$ reproduces (12). To obtain the two-point function in the standard cylindrical coordinates, one instead uses the parametrization $P(t, \phi) = (\sin t, \cos t, \cos \phi, \sin \phi)$.

Comparison to (13) indicates we should choose the $n = \pm 1$ solution, as explained in Appendix A. Without loss of generality, we choose the time-ordered configuration $n = 1$, as choosing $n = -1$ is equivalent to swapping y_1, y_2 , which gives the same geodesic upon extremization.

$$\mathbf{t}_1 - \mathbf{t}_2 = \pi, \quad \mathbf{r}_1 = -\mathbf{r}_2 \quad (17)$$

gives $L = i\pi$. The two bulk endpoints are timelike separated with proper time $\ell_t = \pi$ between them.

Next, we extremize the total length ℓ_s of two spacelike segments that connect (T_i, R_i) with each endpoint of the timelike segment, $(\mathbf{t}_i, \mathbf{r}_i, \boldsymbol{\eta}_i = 0)$,

$$\begin{aligned} \ell_s &= \log \left[\left(\cos(\mathbf{t}_1 - T_1) \cosh \mathbf{r}_1 \cosh R_1 - \sinh \mathbf{r}_1 \sinh R_1 \right) \right. \\ &\quad \left. \times \left(-\cos(\mathbf{t}_1 - T_2) \cosh \mathbf{r}_1 \cosh R_2 + \sinh \mathbf{r}_1 \sinh R_2 \right) / \delta^2 \right]. \end{aligned} \quad (18)$$

Simplifying the expressions obtained by extremizing via $d\ell_s/d\mathbf{t}_1 = d\ell_s/d\mathbf{r}_1 = 0$ gives

$$\begin{aligned} 0 &= \cosh^2 R_1 \sin^2(\mathbf{t}_1 - T_1) - \cosh^2 R_2 \sin^2(\mathbf{t}_1 - T_2), \\ \tanh \mathbf{r}_1 &= \frac{\sin(2\mathbf{t}_1 - T_1 - T_2)}{\tanh R_1 \sin(\mathbf{t}_1 - T_2) + \tanh R_2 \sin(\mathbf{t}_1 - T_1)}. \end{aligned} \quad (19)$$

We have checked numerically for a variety of (T_i, R_i) that there is a unique choice of $(\mathbf{t}_1, \mathbf{r}_1)$ with $\text{Im}(\ell_s) = 0$. In all cases, we find that $\ell_s + i\ell_t = \ell$, where ℓ is given in (13). This agrees with the length extracted from the two-point function, as advertised.

A simple example is the $R_1 = R_2 = 0$ case. The extremization conditions give

$$\sin^2(\mathbf{t}_1 - T_1) - \sin^2(\mathbf{t}_1 - T_2) = 0, \quad \tanh \mathbf{r}_1 = 0. \quad (20)$$

The appropriate solution is

$$\mathbf{t}_1 = \frac{\pi}{2} + \frac{T_1 + T_2}{2}, \quad \mathbf{t}_2 = -\frac{\pi}{2} + \frac{T_1 + T_2}{2}, \quad \mathbf{r}_1 = \mathbf{r}_2 = 0. \quad (21)$$

The special case $T_2 = -T_1$ was studied in [36, 37].

In [36, 37], $n = 1$ was chosen and $\eta = 0$ imposed, although justification for these choices was not provided. The prescription we used derives these conditions. Our prescription is a partial refinement of [36, 37], as we work in the original geometry rather than the Wick-rotated setup, we include an $i\epsilon$ prescription to specify an analytic continuation, and we compare to the analytically continued spacelike length to fix degeneracies.

The prescription we used could have failed upon extremization, as there could have been no segments with real length that solved the constraints. Its success therefore appears to be a non-trivial check. We also applied our approach for arbitrary boundary points, going beyond the specific, symmetric boundary configuration $T_2 = -T_1, R_1 = R_2 = 0$ studied in [36, 37]. See Appendix A for an analysis of the geodesics themselves.

IV. BTZ

We next apply our extremization procedure to the non-rotating BTZ black hole in Kruskal coordinates (u, v, ϕ) . The relation to AdS₃ embedding coordinates is

$$\begin{aligned} X^0 &= \frac{u+v}{1+uv}, & X^1 &= \frac{1-uv}{1+uv} \cosh(r_0 \phi), \\ X^3 &= \frac{v-u}{1+uv}, & X^2 &= \frac{1-uv}{1+uv} \sinh(r_0 \phi). \end{aligned} \quad (22)$$

The metric is

$$ds^2 = -\frac{4}{(1+uv)^2} dudv + \frac{(1-uv)^2}{(1+uv)^2} r_0^2 d\phi^2, \quad (23)$$

where $-\infty < u, v < \infty$, and the horizon radius is r_0 . The surfaces $uv = 0$ are the future and past horizons. The conformal boundary is $uv = -1$ and the singularity is $uv = 1$. Regions with $-1 \leq uv < 0$ lie outside the horizon, while regions with $0 < uv \leq 1$ are inside.

The embedding-space distance formula (8) together with (22) gives the geodesic distance between arbitrary points (u_1, v_1, ϕ_1) and (u_2, v_2, ϕ_2) ,

$$\begin{aligned} \cosh L_{\text{BTZ}} &= \\ &= \frac{2(u_1 v_2 + u_2 v_1) + (1 - u_1 v_1)(1 - u_2 v_2) \cosh(r_0(\phi_2 - \phi_1))}{(1 + u_1 v_1)(1 + u_2 v_2)}. \end{aligned} \quad (24)$$

To obtain the spacelike geodesic between boundary points (U_1, V_1, Φ_1) and (U_2, V_2, Φ_2) , we regulate boundary-anchored geodesics by $U_i V_i = -1 + 2\delta$ with $0 < \delta \ll 1$,

$$\ell_{\text{BTZ}} = \log \left[-\frac{V_1^2 + V_2^2 - 2V_1 V_2 \cosh(r_0(\Phi_1 - \Phi_2))}{V_1 V_2 \delta^2} \right]. \quad (25)$$

For purely timelike separation on the boundary ($\Phi_1 = \Phi_2$),

$$\ell_{\text{BTZ}} = i\pi + \log \left(\frac{(V_1 - V_2)^2}{V_1 V_2 \delta^2} \right). \quad (26)$$

We now apply our extremization prescription. With bulk endpoints $(\mathbf{u}_1, \mathbf{v}_1)$ and $(\mathbf{u}_2, \mathbf{v}_2)$, extremizing the length (24) between timelike-separated points gives

$$\begin{aligned} \frac{dL}{du_1} &= -\frac{2(1+u_2 v_1)(v_1 - v_2)}{(1+u_1 v_1)^2(1+u_2 v_2)} = 0, \\ \frac{dL}{du_2} &= \frac{2(v_1 - v_2)(1+u_1 v_2)}{(1+u_1 v_1)(1+u_2 v_2)^2} = 0, \\ \frac{dL}{dv_1} &= -\frac{2(u_1 - u_2)(1+u_1 v_2)}{(1+u_1 v_1)^2(1+u_2 v_2)} = 0, \\ \frac{dL}{dv_2} &= \frac{2(u_1 - u_2)(1+u_2 v_1)}{(1+u_1 v_1)(1+u_2 v_2)^2} = 0. \end{aligned} \quad (27)$$

Comparing to (26) instructs us to exclude the coincident-point solution. The conditions (27) then imply

$$1 + \mathbf{u}_1 \mathbf{v}_2 = 0, \quad 1 + \mathbf{u}_2 \mathbf{v}_1 = 0, \quad (28)$$

for which (24) gives $\cosh L_{\text{BTZ}} = -1$. This confirms these bulk points are timelike separated and that the segment has proper time $\ell_t = \pi$.

Next, we extremize the spacelike segments that connect the bulk points $(\mathbf{u}_i, \mathbf{v}_i)$ with boundary points (U_i, V_i) . In the small δ limit, the length of the spacelike segment is

$$\ell_s = \log \left[-\frac{16(V_1 - \mathbf{v}_1)(V_1 - \mathbf{v}_2)(V_2 - \mathbf{v}_1)(V_2 - \mathbf{v}_2)}{V_1 V_2 (\mathbf{v}_1 - \mathbf{v}_2)^2 \delta^2} \right]. \quad (29)$$

Using (28) to eliminate $(\mathbf{u}_2, \mathbf{v}_2)$, for example, and then extremizing ℓ_s gives

$$\begin{aligned} \frac{d\ell_s}{d\mathbf{u}_1} &= \frac{V_1 + V_2 + 2V_1 V_2 \mathbf{u}_1 - 2\mathbf{v}_1 - (V_1 + V_2)\mathbf{u}_1 \mathbf{v}_1}{(1 + V_1 \mathbf{u}_1)(1 + V_2 \mathbf{u}_1)(1 + \mathbf{u}_1 \mathbf{v}_1)} = 0, \\ \frac{d\ell_s}{d\mathbf{v}_1} &= \frac{V_1 + V_2 + 2V_1 V_2 \mathbf{u}_1 - 2\mathbf{v}_1 - (V_1 + V_2)\mathbf{u}_1 \mathbf{v}_1}{(V_1 - \mathbf{v}_1)(-V_2 + \mathbf{v}_1)(1 + \mathbf{u}_1 \mathbf{v}_1)} = 0. \end{aligned} \quad (30)$$

As the numerators are identical, we have a one-parameter family of solutions, which we parametrize by \mathbf{u}_1 ,

$$\begin{aligned} (\mathbf{u}_1, \mathbf{v}_1) &= \left(\mathbf{u}_1, \frac{V_1 + V_2 + 2V_1 V_2 \mathbf{u}_1}{2 + \mathbf{u}_1(V_1 + V_2)} \right), \\ (\mathbf{u}_2, \mathbf{v}_2) &= \left(-\frac{2 + \mathbf{u}_1(V_1 + V_2)}{V_1 + V_2 + 2V_1 V_2 \mathbf{u}_1}, -\frac{1}{\mathbf{u}_1} \right). \end{aligned} \quad (31)$$

To determine where these points reside, we check the range of $s_1 \equiv \mathbf{u}_1 \mathbf{v}_1$ and $s_2 \equiv \mathbf{u}_2 \mathbf{v}_2$. From (31), we see that $s_1 s_2 = 1$. However, only points satisfying $-1 \leq s_1, s_2 \leq 1$ lie within the BTZ geometry. The only allowed values are therefore $s_1 = s_2 = 1$, meaning the two endpoints are on the singularities. Imposing this condition fixes $\mathbf{u}_1^2 = 1/(V_1 V_2)$. The time-ordered configuration is where $(\mathbf{u}_1, \mathbf{v}_1)$ lies on the future singularity, or $\mathbf{u}_1 = 1/\sqrt{V_1 V_2}$. This agrees with [36, 37], which imposed that the endpoints were affixed to the singularities but without providing a justification. We therefore have

$$\ell_s = \log \frac{(V_1 - V_2)^2}{V_1 V_2 \delta^2}. \quad (32)$$

The total complex length $\ell_s + i\ell_t$ precisely reproduces the boundary result (26).

The Euclidean thermal two-point function on the cylinder parametrized by (x, τ) at inverse temperature β is

$$\langle 0 | \mathcal{O}(x, \tau) \mathcal{O}(0) | 0 \rangle = \left(\frac{(\pi/\beta)^2}{\sinh \frac{\pi}{\beta}(x + i\tau) \sinh \frac{\pi}{\beta}(x - i\tau)} \right)^\Delta. \quad (33)$$

We analytically continue to the Lorentzian configuration $\tau = i(T_2 - T_1)$, $x = 0$, and the length extracted from the

resulting correlator is equal to the quantity $\ell_s + i\ell_t$ we computed, upon substituting $V_i = e^{r_0 T_i}$ and $\beta = 2\pi/r_0$.

In Appendix B, we show that in fact a continuous family of geodesics connects the bulk points we identified, all with the same total length ℓ . One but not all of them lie entirely behind the horizon.

V. FUTURE DIRECTIONS

Composite geodesics and their relationship with CFT correlators warrant a more systematic study. Computing CFT correlators in the WKB regime [29] or using world-line methods [41] may lead to an unambiguous derivation of universal rules for computing composite geodesics. We expect this will clarify whether having a multiplicity of bulk geodesics is an intrinsic feature similar to the non-isometric encoding of infalling observers [7], or a sign the prescription needs further refinement. Studying these ideas in correlators of heavy operators [42] may help identify technically natural CFT definitions of an observer and the bulk worldline on-shell action. A geodesic Witten diagram construction for timelike separations may be relevant here [43].

Our work and [36, 37] only studied examples in which the proper time ℓ_t was π . Setups with other values of ℓ_t would be useful for exploring ℓ_t as a manifestly

diffeomorphism-invariant notion of bulk observer time. For related work on proper distance and time correlators in gravity, see [8, 44–47].

Our results suggest new ways to understand time-like entanglement entropy [36–38]. In AdS₃/CFT₂ one may attempt to derive a bulk prescription by applying our methods to twist operators analytically continued to timelike separations. A possibly related connection between entropy and CFT correlators is the equivalence between the modular Hamiltonian and the stress-tensor OPE block [32, 33, 35, 48].

ACKNOWLEDGMENTS

We thank Yanbei Chen, Sumit Das, Per Kraus, Jonathan Harper, David Poland, Mohamed Radwan, Gordon Rogelberg, and Alfred Shapere for discussions and comments on the draft. During this work, AS has been supported by the Heising-Simons Foundation “Observational Signatures of Quantum Gravity” collaboration grant 2021-2817; by the D.O.E., Office of High Energy Physics, under Award No. DE-SC0011632; and by the Walter Burke Institute for Theoretical Physics. HB is partially supported by the National Science Foundation grants NSF-PHY/211673 and NSF-PHY/2410647.

-
- [1] A. Hamilton, D. N. Kabat, G. Lifschytz, and D. A. Lowe, “Holographic representation of local bulk operators,” *Phys. Rev. D* **74** (2006) 066009, [arXiv:hep-th/0606141](#).
- [2] D. Kabat, G. Lifschytz, and D. A. Lowe, “Constructing local bulk observables in interacting AdS/CFT,” *Phys. Rev. D* **83** (2011) 106009, [arXiv:1102.2910 \[hep-th\]](#).
- [3] S. Ryu and T. Takayanagi, “Holographic derivation of entanglement entropy from AdS/CFT,” *Phys. Rev. Lett.* **96** (2006) 181602, [arXiv:hep-th/0603001](#).
- [4] D. Harlow, “TASI Lectures on the Emergence of Bulk Physics in AdS/CFT,” *PoS TASI2017* (2018) 002, [arXiv:1802.01040 \[hep-th\]](#).
- [5] K. Papadodimas and S. Raju, “An Infalling Observer in AdS/CFT,” *JHEP* **10** (2013) 212, [arXiv:1211.6767 \[hep-th\]](#).
- [6] K. Papadodimas and S. Raju, “State-Dependent Bulk-Boundary Maps and Black Hole Complementarity,” *Phys. Rev. D* **89** no. 8, (2014) 086010, [arXiv:1310.6335 \[hep-th\]](#).
- [7] C. Akers, N. Engelhardt, D. Harlow, G. Penington, and S. Vardhan, “The black hole interior from non-isometric codes and complexity,” *JHEP* **06** (2024) 155, [arXiv:2207.06536 \[hep-th\]](#).
- [8] S. B. Giddings, “Quantum gravity observables: observation, algebras, and mathematical structure*,” *J. Phys. A* **58** no. 41, (2025) 415401, [arXiv:2505.22708 \[hep-th\]](#).
- [9] M. Gary, S. B. Giddings, and J. Penedones, “Local bulk S-matrix elements and CFT singularities,” *Phys. Rev. D* **80** (2009) 085005, [arXiv:0903.4437 \[hep-th\]](#).
- [10] J. Polchinski, L. Susskind, and N. Toumbas, “Negative energy, superluminality and holography,” *Phys. Rev. D* **60** (1999) 084006, [arXiv:hep-th/9903228](#).
- [11] I. Heemskerk, J. Penedones, J. Polchinski, and J. Sully, “Holography from Conformal Field Theory,” *JHEP* **10** (2009) 079, [arXiv:0907.0151 \[hep-th\]](#).
- [12] J. Penedones, “Writing CFT correlation functions as AdS scattering amplitudes,” *JHEP* **03** (2011) 025, [arXiv:1011.1485 \[hep-th\]](#).
- [13] T. Okuda and J. Penedones, “String scattering in flat space and a scaling limit of Yang-Mills correlators,” *Phys. Rev. D* **83** (2011) 086001, [arXiv:1002.2641 \[hep-th\]](#).
- [14] J. Maldacena, D. Simmons-Duffin, and A. Zhiboedov, “Looking for a bulk point,” *JHEP* **01** (2017) 013, [arXiv:1509.03612 \[hep-th\]](#).
- [15] O. Aharony, L. F. Alday, A. Bissi, and E. Perlmutter, “Loops in AdS from Conformal Field Theory,” *JHEP* **07** (2017) 036, [arXiv:1612.03891 \[hep-th\]](#).
- [16] D. Meltzer, E. Perlmutter, and A. Sivaramakrishnan, “Unitarity Methods in AdS/CFT,” *JHEP* **03** (2020) 061, [arXiv:1912.09521 \[hep-th\]](#).
- [17] D. Meltzer and A. Sivaramakrishnan, “CFT unitarity and the AdS Cutkosky rules,” *JHEP* **11** (2020) 073, [arXiv:2008.11730 \[hep-th\]](#).
- [18] S. Caron-Huot, J. Chakravarty, and K. Namjou, “Boundary imprint of bulk causality,” *JHEP* **07** (2025) 076, [arXiv:2501.13182 \[hep-th\]](#).
- [19] S. Caron-Huot, J. Chakravarty, and K. Namjou,

- “Looking at bulk points in general geometries,” [arXiv:2502.14963 \[hep-th\]](#).
- [20] G. Festuccia and H. Liu, “Excursions beyond the horizon: Black hole singularities in Yang-Mills theories. I.,” *JHEP* **04** (2006) 044, [arXiv:hep-th/0506202](#).
- [21] V. E. Hubeny, H. Liu, and M. Rangamani, “Bulk-cone singularities & signatures of horizon formation in AdS/CFT,” *JHEP* **01** (2007) 009, [arXiv:hep-th/0610041](#).
- [22] G. Festuccia and H. Liu, “A Bohr-Sommerfeld quantization formula for quasinormal frequencies of AdS black holes,” *Adv. Sci. Lett.* **2** (2009) 221–235, [arXiv:0811.1033 \[gr-qc\]](#).
- [23] P. Kraus, H. Ooguri, and S. Shenker, “Inside the horizon with AdS / CFT,” *Phys. Rev. D* **67** (2003) 124022, [arXiv:hep-th/0212277](#).
- [24] N. Čeplak, H. Liu, A. Parnachev, and S. Valach, “Black hole singularity from OPE,” *JHEP* **10** (2024) 105, [arXiv:2404.17286 \[hep-th\]](#).
- [25] M. Grinberg and J. Maldacena, “Proper time to the black hole singularity from thermal one-point functions,” *JHEP* **03** (2021) 131, [arXiv:2011.01004 \[hep-th\]](#).
- [26] N. Afkhami-Jeddi, S. Caron-Huot, J. Chakravarty, and A. Maloney, “Imprint of the black hole singularity on thermal two-point functions,” [arXiv:2510.21673 \[hep-th\]](#).
- [27] N. Čeplak, H. Liu, A. Parnachev, and S. Valach, “Fooling the Censor: Going beyond inner horizons with the OPE,” [arXiv:2511.09638 \[hep-th\]](#).
- [28] M. Dodelson, C. Iossa, and R. Karlsson, “Bouncing off a stringy singularity,” [arXiv:2511.09616 \[hep-th\]](#).
- [29] V. Balasubramanian, A. Bernamonti, B. Craps, V. Keränen, E. Keski-Vakkuri, B. Müller, L. Thorlacius, and J. Vanhoof, “Thermalization of the spectral function in strongly coupled two dimensional conformal field theories,” *JHEP* **04** (2013) 069, [arXiv:1212.6066 \[hep-th\]](#).
- [30] I. Y. Aref’eva, M. A. Khramtsov, and M. D. Tikhonovskaya, “Improved image method for a holographic description of conical defects,” *Theor. Math. Phys.* **189** no. 2, (2016) 1660–1672, [arXiv:1604.08905 \[hep-th\]](#).
- [31] J.-H. He and R.-Q. Yang, “Geodesics connecting endpoints of timelike interval in an asymptotically AdS spacetime,” *Phys. Rev. D* **111** no. 2, (2025) 026024, [arXiv:2408.04783 \[hep-th\]](#).
- [32] B. Czech, L. Lamprou, S. McCandlish, B. Mosk, and J. Sully, “Equivalent Equations of Motion for Gravity and Entropy,” *JHEP* **02** (2017) 004, [arXiv:1608.06282 \[hep-th\]](#).
- [33] B. Czech, L. Lamprou, S. McCandlish, B. Mosk, and J. Sully, “A Stereoscopic Look into the Bulk,” *JHEP* **07** (2016) 129, [arXiv:1604.03110 \[hep-th\]](#).
- [34] G. Sárosi and T. Ugajin, “Modular Hamiltonians of excited states, OPE blocks and emergent bulk fields,” *JHEP* **01** (2018) 012, [arXiv:1705.01486 \[hep-th\]](#).
- [35] F. M. Haehl and K.-W. Huang, “Virasoro OPE Blocks, Causal Diamonds, and Higher-Dimensional CFT,” [arXiv:2505.12456 \[hep-th\]](#).
- [36] K. Doi, J. Harper, A. Mollabashi, T. Takayanagi, and Y. Taki, “Pseudoentropy in dS/CFT and Timelike Entanglement Entropy,” *Phys. Rev. Lett.* **130** no. 3, (2023) 031601, [arXiv:2210.09457 \[hep-th\]](#).
- [37] K. Doi, J. Harper, A. Mollabashi, T. Takayanagi, and Y. Taki, “Timelike entanglement entropy,” *JHEP* **05** (2023) 052, [arXiv:2302.11695 \[hep-th\]](#).
- [38] A. Milekhin, Z. Adamska, and J. Preskill, “Observable and computable entanglement in time,” [arXiv:2502.12240 \[quant-ph\]](#).
- [39] M. P. Heller, F. Ori, and A. Serantes, “Geometric Interpretation of Timelike Entanglement Entropy,” *Phys. Rev. Lett.* **134** no. 13, (2025) 131601, [arXiv:2408.15752 \[hep-th\]](#).
- [40] M. P. Heller, F. Ori, and A. Serantes, “Temporal Entanglement from Holographic Entanglement Entropy,” *Phys. Rev. X* **15** no. 4, (2025) 041022, [arXiv:2507.17847 \[hep-th\]](#).
- [41] H. Maxfield, “A view of the bulk from the worldline,” [arXiv:1712.00885 \[hep-th\]](#).
- [42] D. Poland and G. Rogelberg, “Moments and saddles of heavy CFT correlators,” [arXiv:2501.00092 \[hep-th\]](#).
- [43] E. Hijano, P. Kraus, E. Perlmutter, and R. Snively, “Witten Diagrams Revisited: The AdS Geometry of Conformal Blocks,” *JHEP* **01** (2016) 146, [arXiv:1508.00501 \[hep-th\]](#).
- [44] A. Almheiri, A. Goel, and X.-Y. Hu, “Quantum gravity of the Heisenberg algebra,” *JHEP* **08** (2024) 098, [arXiv:2403.18333 \[hep-th\]](#).
- [45] L. V. Iliesiu, A. Levine, H. W. Lin, H. Maxfield, and M. Mezei, “On the non-perturbative bulk Hilbert space of JT gravity,” *JHEP* **10** (2024) 220, [arXiv:2403.08696 \[hep-th\]](#).
- [46] D. Carney, M. Karydas, and A. Sivaramakrishnan, “Response of interferometers to the vacuum of quantum gravity,” [arXiv:2409.03894 \[hep-th\]](#).
- [47] A. Sivaramakrishnan, “Observer Time from Causality in Perturbative Quantum Gravity,” [arXiv:2506.16109 \[hep-th\]](#).
- [48] M. W. Bub and A. Sivaramakrishnan, “Correlation functions of von Neumann entropy,” [arXiv:2506.10917 \[hep-th\]](#).
- [49] D. L. Jafferis and L. Lamprou, “Inside the hologram: reconstructing the bulk observer’s experience,” *JHEP* **03** (2022) 084, [arXiv:2009.04476 \[hep-th\]](#).
- [50] J. de Boer, D. L. Jafferis, and L. Lamprou, “On black hole interior reconstruction, singularities and the emergence of time,” [arXiv:2211.16512 \[hep-th\]](#).
- [51] S. A. W. Leutheusser and H. Liu, “Emergent Times in Holographic Duality,” *Phys. Rev. D* **108** no. 8, (2023) 086020, [arXiv:2112.12156 \[hep-th\]](#).

Appendix A: Geodesic method for global AdS₃

We derive (17) using geodesic equations in AdS₃ for boundary points at the same angular location ($\Phi_1 = \Phi_2$). We float the bulk endpoints and impose constraints to fix the timelike and spacelike segments.

First we study the timelike segment. In global coordinates, the velocities obey

$$-(\cosh^2 \rho) \dot{\tau}^2 + \dot{\rho}^2 + (\sinh^2 \rho) \dot{\phi}^2 = -1, \quad (\text{A1})$$

and the conserved quantities along a geodesic are

$$(\cosh^2 \rho) \dot{\tau} = P_\tau, \quad (\sinh^2 \rho) \dot{\phi} = P_\phi, \quad (\text{A2})$$

with radial equation

$$\dot{\rho}^2 = -1 + P_\tau^2 \operatorname{sech}^2 \rho - P_\phi^2 \operatorname{csch}^2 \rho. \quad (\text{A3})$$

Restricting to constant- ϕ solutions ($P_\phi = 0$), the turning point ρ_* obeys $P_\tau = \cosh \rho_*$. The proper time between endpoints (τ_1, ρ_1) and (τ_2, ρ_2) is

$$\ell_t = \int d\lambda = \left\{ \int_{\rho_1}^{\rho_*} + \int_{\rho_2}^{\rho_*} \right\} \frac{d\rho}{\sqrt{-1 + P_\tau^2 \operatorname{sech}^2 \rho}}, \quad (\text{A4})$$

which is maximized by $\rho_1 = \rho_2 = 0$, yielding $\ell_t = \pi$. The entire timelike segment then sits at $\rho = 0$ with $P_\tau = 1$ and the endpoints satisfy $\tau_1 - \tau_2 = \pi$.

Next we study the spacelike segment, still imposing $P_\phi = 0$. For the spacelike legs that connect $(\rho = 0, \tau_{1,2})$ to boundary points $(\rho_\infty, T_{1,2})$,

$$-(\cosh^2 \rho) \dot{\tau}^2 + \dot{\rho}^2 = 1, \quad c_\tau \equiv (\cosh^2 \rho) \dot{\tau} \quad (\text{A5})$$

Boundary conditions fix

$$\tau_1 = \frac{\pi}{2} + \bar{T}_0, \quad \tau_2 = -\frac{\pi}{2} + \bar{T}_0, \quad (\text{A6})$$

$$c_\tau = \cot\left(\frac{T_1 - T_2}{2}\right), \quad \bar{T}_0 = \frac{T_1 + T_2}{2}. \quad (\text{A7})$$

The regulated length of the two spacelike legs is

$$\ell_s = \int_0^{\rho_\infty} \frac{2 d\rho}{\sqrt{1 + c_\tau^2 \operatorname{sech}^2 \rho}} = \log \left[\frac{\sin^2\left(\frac{T_1 - T_2}{2}\right)}{\delta^2} \right], \quad (\text{A8})$$

with $\delta = e^{-\rho_\infty} \ll 1$.

Note that ℓ_t at $\rho = 0$ is monotonically increasing in the separation between endpoints, as evident from (A2) with $P_\tau = 1$ and $\rho = 0$.

Appendix B: Geodesic Calculation for BTZ

Here we rederive (28) using geodesic equations in the BTZ geometry. Let dots denote $d/d\lambda$ and primes d/dv .

The nontrivial affine geodesic equations for (23) with $\dot{\phi} = 0$ are

$$\ddot{u} - \frac{2v}{1+uv} \dot{u}^2 = 0, \quad \ddot{v} - \frac{2u}{1+uv} \dot{v}^2 = 0. \quad (\text{B1})$$

Parameterizing the curve as $u(v)$ gives

$$(1+uv)u'' + 2(u-vu')u' = 0, \quad (\text{B2})$$

whose general solution is

$$u(v) = \frac{a+bv}{1+av}, \quad (\text{B3})$$

with real constants a, b . Along (B3), the induced line element is

$$ds^2 = -\frac{4}{(1+uv)^2} u'(v) dv^2 = \frac{4(a^2-b)dv^2}{(1+2av+bv^2)^2}. \quad (\text{B4})$$

The curve is spacelike for $a^2 - b > 0$ and timelike for $a^2 - b < 0$. When $a^2 > b$ there are two turning points,

$$v_\pm = \frac{-a}{b} \pm \sqrt{\frac{a^2}{b} - 1}, \quad (\text{B5})$$

whereas for $a^2 - b < 0$, v_\pm are complex and $u(v)$ is monotonic. For timelike separated bulk endpoints (u_1, v_1) and (u_2, v_2) , define

$$y(v) = \frac{a+bv}{\sqrt{-a^2+b}}. \quad (\text{B6})$$

The proper time for this curve is then given as

$$\ell_t = \int_{v_1}^{v_2} dv \frac{2\sqrt{-a^2+b}}{1+2av+bv^2} = 2 \tan^{-1} \left[\frac{y_2 - y_1}{1 + y_1 y_2} \right], \quad (\text{B7})$$

which is maximized when $1 + y_1 y_2 = 0$ with $\ell_t = \pi$. Using (B3), this condition is equivalent to

$$v_2 = -\frac{1+av_1}{a+bv_1} = -\frac{1}{u_1}, \quad v_1 = -\frac{1+av_2}{a+bv_2} = -\frac{1}{u_2}, \quad (\text{B8})$$

precisely matching (28).

As a special case, we will consider the configuration with one endpoint on the future singularity. Choose $(u_1, v_1) = (1/v_+, v_+)$ with $v_+ > 0$ (so $u_1 v_1 = 1$). From (B3),

$$\frac{1}{v_+} = \frac{a+bv_+}{1+av_+} \Rightarrow b = \frac{1}{v_+^2}. \quad (\text{B9})$$

The length is given by (B7), with endpoints fixed by $uv = 1$. Let the corresponding v -values be v_\pm ; then

$$v_\pm = \pm \frac{1}{\sqrt{b}}, \quad y_+ y_- = -1, \quad \ell_t = \pi. \quad (\text{B10})$$

The timelike segment is therefore

$$u_t(v) = \frac{a+v/v_+^2}{1+av}, \quad (\text{B11})$$

with $v_+ > 0$ and $a \in (-1/v_+, 1/v_+)$. All such curves have the same length $i\pi$. Extremizing the spacelike legs fixes $v_+ = \sqrt{V_1 V_2}$ as also shown in Section IV, while a remains free within $|a| < 1/v_+$. Only the curve with $a = 0$ crosses the bifurcate horizon. For $a \neq 0$, the timelike curve $u_t(v)$ leaves the $u = 0$ horizon at $(u, v) = (0, -av_+^2)$, enters the right wedge, and re-enters the $v = 0$ horizon at $(u, v) = (a, 0)$. For future-directed curves, $a = 0$.

Appendix C: Proper time vs. modular time

We have focused on reconstructing the proper time of bulk timelike geodesics. Other methods of reconstructing bulk time use modular flow [49–51] and are connected to geodesic time only in special cases. However, it is important to note that aside from the special case of Rindler, modular time is different from time experienced by an inertial observer. The former is a formal notion of time that exists for any state, while the latter is what appears more naturally in experiment and requires some well-defined clock. This distinction may be crucial for the holographic reconstruction of bulk time, and so we make this comparison explicit here.

In the right Rindler wedge of Minkowski space, the modular Hamiltonian is the boost generator. Under the conformal map that sends the wedge to the causal diamond $D(B_R)$ of a ball of radius R , the modular flow

becomes the conformal Killing field, which in $(1+1)$ dimensions is

$$\zeta_B = \frac{\pi}{R} \left[(R^2 - t^2 - x^2) \partial_t - 2tx \partial_x \right]. \quad (\text{C1})$$

Integral curves $(t(\lambda), x(\lambda))$ of ζ_B obey

$$\frac{dt}{dx} = \frac{-R^2 + t^2 + x^2}{2tx}, \quad (\text{C2})$$

and can be written equivalently as the one-parameter family of hyperbolae labeled by a constant ξ_0 ,

$$\frac{t^2 - (R+x)^2}{t^2 - (R-x)^2} = \frac{\xi_0^2}{4R^2}, \quad (\text{C3})$$

which furnishes a convenient check of (C2). Note that dx/dt is not constant, indicating the trajectory is non-inertial. The relation between modular time η and t is

$$\eta(t, x) = \tanh^{-1} \left(\frac{2Rt}{R^2 + t^2 - x^2} \right). \quad (\text{C4})$$

It is easy to check that for $x = 0$, the observer is inertial, and furthermore that modular time is non-linearly related to proper time. Modular time is therefore not directly measurable by the clock of some observer in this setup.